

Topological extension including quantum jump

Xiangyu Niu¹ and Junjie Wang¹

¹*Center for Quantum Sciences, School of Physics, Northeast Normal University, Changchun 130024, China.**

(Dated: December 7, 2022)

We study the topological properties of the Su-Schrieffer-Heeger (SSH) model with collective loss and gain, by using the technique of the third quantization to the Lindblad master equation. With the help of the generalized Brillouin zone (GBZ) theory, it allows one to study the topological properties through the shape matrix in the presence or absence of the quantum jumping terms. Among which the latter case is dynamically equivalent to a fully studied non-reciprocal non-Hermitian (NH) SSH model. It is clear that they share the same transition points, and the definition of the corresponding winding number is given out. In addition, when the quantum jumping terms are presented, the phase transition points may shift, which cannot be predicted by the effective non-Hermitian theory. Our work bridges the NH and open quantum system descriptions in studying the topological properties, and reveals the unique role of quantum jumps.

I. INTRODUCTION

Topological band theory has always played an important role in various fields of quantum physics and material science. Recently, the related researches have gradually moved into non-Hermitian regime [1], and have evoked extreme repercussions [2–8]. However, some behaviors that are well-studied in Hermitian systems are challenged when moving to the NH regime. For example, for quite a long time, the bulk-boundary correspondence, which builds the bridge between the edge states and bulk topological invariant, encounters difficulties in NH systems [9–12]. Fortunately, the establishment of generalized Brillouin zone theory solves this problem to some extent [2, 13]. It indicates that the usually used Brillouin zone (BZ) in Hermitian systems may break down. Instead, the corresponding wave number k becomes complex in general, and the trajectory of $\beta = e^{ik}$ in the complex plane is called the generalized Brillouin zone. The establishment of GBZ theory makes it possible to predict the bulk-boundary correspondence as well as the transition points in some of the NH systems, which also opens the gate for further studies.

One of the essential implementations of non-Hermiticity is through the open quantum system, among all the open descriptions, the Lindblad markov master equation is definitely the most reliable and commonly used theory [14]. By solving the evolution of the density operator over time, it is possible to track the changes of energy, information, and coherence of the system, etc. However, no matter studying the density operator or the Liouvillian operator that is extended from the master equation [15], the calculation cost will be the square of the system Hilbert space dimension, and significantly increases the difficulty of the study. In most cases, only numerical solutions can be given out, especially for complicated many body systems. Comparatively, the NH approach provides a simpler description of dissipation, and can substitute for the master equation dynamic to some extent. When the jumping terms in the master equation, which represent the stochastic jumps, are neglected, the dynamic is just the same as the NH ones. Actually, many NH systems in a series of works are indeed intro-

duced based on this principle [4, 5, 16]. However, the quantum jumping terms may be non-negligible in many cases, because they could induce interesting phenomena or differences [15, 17]. From the point view of the wave function, it may commit abrupt perturbation [18, 19], or influence the spectrum of Liouvillian operator [15, 17, 20]. Given that both descriptions have established a series of theoretical frameworks, exploring their similarities and differences has drawn increasing attention in recent years [21–23]. Among them, the extension of topological phase in open quantum system is a particularly urgent task, but is still in its infancy [24–27]. Naturally, one may wonder how the quantum jumping terms could affect the topological properties. Here, we will address the above issues and show the effect of quantum jumps through a specific model.

In this paper, we mainly concentrate on a NH SSH model studied in Ref. [2] as an example, which has a pair of asymmetric hopping terms in the unit cell. The difference is that its implementation is through the Lindblad master equation with collective loss and gain, and when all the jumping terms are ignored, they are dynamically equivalent. With the help of the third quantization technique and the GBZ theory, we deduce the shape matrix and study their topological properties both when the quantum jumping terms are absent or presented. By comparing with the effective approach, when no quantum jumps occur, the results show that they share the same transition points, which illustrates the validity of our scheme. Furthermore, we analyze the circumstances including the quantum jumping terms similarly. The results show that the transition points may be shifted and the symmetry of the shape matrix changes. It reveals that the quantum jump may have unique role in topological systems, and should be carefully examined. Our work paves the way for defining the topological phase, which is a challenge of current researches.

This paper is organized as follows. In Sec. II we present the example model of the entire paper and introduce the basic theory, third quantization, to derive the shape matrix. In Sec. III we classify the symmetries of the model either with or without quantum jump. In Sec. IV we apply the auxiliary GBZ theory to calculate the GBZ, and define the topological invariants of both descriptions in Sec. V, we also briefly discuss the preserving of bulk-boundary correspondence. Finally, in Sec. VI

* niuxy795@nenu.edu.cn

we conclude and dampen expectations.

II. MODEL

In this section, we start from a one-dimension SSH lattice with dissipation, as shown in Fig. 1(a). The internal hopping strength between sites A and sites B is t_1 , and the strength between the neighbor cells is t_2 . The free Hamiltonian H can be written as $H = \sum_n^{N/2} (t_1 c_{nA}^\dagger c_{nB} + t_2 c_{n+1A}^\dagger c_{nB} + \text{H.c.})$, where c is the annihilation operator of fermion and the subscript denotes the site A,B in the n th unit cell.

Considering the system is suffering loss and gain, it is convenient to be presented by the Lindblad master equation [14]

$$\mathcal{L}\rho = \dot{\rho} = -i[H, \rho] + \sum_{\mu} (2\kappa L_{\mu}\rho L_{\mu}^\dagger - \rho L_{\mu}^\dagger L_{\mu} - L_{\mu}^\dagger L_{\mu}\rho), \quad (1)$$

where \mathcal{L} is the Liouvillian superoperator. Terms shaped as $L_{\mu}\rho L_{\mu}^\dagger$ are usually called jumping terms, equivalent to the continuous measurements to the system induced by the environment. Here we add a real index κ as the quantum jump parameter, which characterizes the strength that the jump occurs. Such structure is named as “hybrid Liouvillian” in Ref. [28]. In this work, we mainly focus on two common cases, the first is $\kappa = 1$ for the full dynamic of the master equation and the second is $\kappa = 0$. The latter case is often discussed in many works. For instance, when the system is considered at a specific time scale that is sufficiently small compared with the inverse loss rate $1/\gamma$ [29], whereas in other works, the authors may choose to perform post-selected operations [30] or assume loss processes of a coherent condensate [31]. After the following procedures, they assume that the jumping terms in the master equation can be safely neglected, and the system is governed by an effective NH Hamiltonian

$$H_{eff} = H - \frac{i}{2} \sum_{\mu} L_{\mu}^\dagger L_{\mu}. \quad (2)$$

Back to our model, the Lindblad operators L_{μ} include

$$L_{1,n} = \sqrt{\gamma_l}(c_{nA} + ic_{nB}), \quad (3a)$$

$$L_{2,n} = \sqrt{\gamma_g}(c_{nA}^\dagger + ic_{nB}^\dagger), \quad (3b)$$

where $L_{1,n}$ stands for the collective loss and $L_{2,n}$ represents the gain, the γ_l, γ_g are the rates of loss and gain. These types of dissipation can also be found in Ref. [21, 32–34]. Without loss of generality, we assume $t_1, t_2, \gamma_l, \gamma_g$ are all real. When the jumping terms are absent ($\kappa = 0$), it is straightforward to find that the effective Hamiltonian H_{eff} in Eq. (2) takes

$$H_{eff} = \sum_n ((t_1 + \frac{\gamma}{2})c_{nA}^\dagger c_{nB} + (t_1 - \frac{\gamma}{2})c_{nB}^\dagger c_{nA} + t_2(c_{n+1A}^\dagger c_{nB} + c_{nB}^\dagger c_{n+1A}) - \frac{i}{2}\gamma'(c_{nA}^\dagger c_{nA} + c_{nB}^\dagger c_{nB})), \quad (4)$$

here $\gamma = \gamma_l + \gamma_g$, $\gamma' = \gamma_l - \gamma_g$. Actually, the overall loss $-i\gamma'/2$ is negligible because $N = \sum_n (c_{nA}^\dagger c_{nA} + c_{nB}^\dagger c_{nB})$ is the

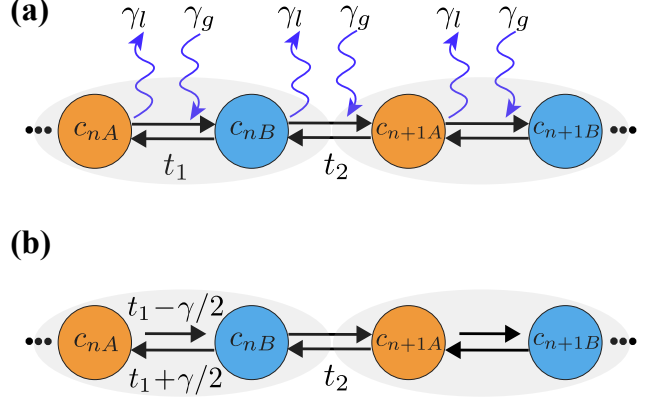


FIG. 1. (a) The SSH lattice with intrinsic staggered hopping as well as loss and gain, the total number of sites is N . The intracell hopping strength is t_1 , the intercell hopping is t_2 , and the strength of collective loss and gain is γ_l and γ_g . When the quantum jump is absent, the dynamic is equivalent to (b), an effective non-reciprocal SSH model with hopping $t_1 \pm \gamma/2$, $\gamma = \gamma_l + \gamma_g$.

total particle number of the system, which can be viewed as a constant. Concisely, it is the same as Fig. 1(b), which is exactly the model studied in Ref. [2], the GBZ and corresponding topological invariant is defined and calculated. The results show that it can precisely predict the transition points, and the consistency between the edge states and winding number implies the establishment of new bulk-boundary correspondence in 1D non-Hermitian systems.

The third quantization

It is natural to ask, what may happen if the jumping terms $L_{\mu}\rho L_{\mu}^\dagger$ for any μ could not be neglected. However, this problem can become very difficult, since taking the jumping terms into consideration will result in a rapid increase in matrix dimensionality $\propto N^2$ [15]. For such quadratic fermionic dissipative systems, by applying the third quantization established by Prosen *et al.* [35], the dimension could be reduced to $4N$, which will be useful for afterwards studies. We begin by transforming the model in terms of the Majorana operators

$$w_{2m-1} = c_m + c_m^\dagger, w_{2m} = i(c_m - c_m^\dagger), \quad (5)$$

which satisfies the anticommutation relations $\{w_m, w_n\} = 2\delta_{mn}$. Under this basis, the free Hamiltonian H and Lindblad operators can be represented as $H = \sum_{jk} w_j H_{j,k} w_k$ and $L_{\mu} = \sum_{\mu} l_{\mu,j} w_j$. After mapping the Liouvillian operator \mathcal{L} into the Liouvillian-fork space [36, 37], we can define the creation and annihilation operators \hat{c}_j^\dagger and \hat{c}_j as (named as “a-fermions”, we use the “hat” for distinction)

$$\hat{c}_j|P_{\alpha}\rangle = \delta_{\alpha,j,1}|w_j P_{\alpha}\rangle, \hat{c}_j^\dagger|P_{\alpha}\rangle = \delta_{\alpha,j,0}|w_j P_{\alpha}\rangle, \alpha_j \in \{0, 1\}, \quad (6)$$

here the density matrix ρ is vectorized to a linear combination of the 2^{2N} polynomials $P_{\alpha} = w_1^{\alpha_1} w_2^{\alpha_2} \dots w_{2n}^{\alpha_{2n}}$. The $|P_{\alpha}\rangle$ is the

corresponding canonical basis of the vector space, and the inner product satisfies $\langle x|y \rangle = 4^{-N} \text{tr} x^\dagger y$. By using Eq. (6) and substitute back to Eq. (1), after some mathematical calculations, we can obtain the each part of the Lindblad maps, and will be shown below.

The Liouvillian \mathcal{L} can be split into $\mathcal{L} = \mathcal{L}_0 + \mathcal{L}_{diss}$, the first part $\mathcal{L}_0 \rho := -i[H, \rho]$ describes the unitary evolution, which is governed by the free Hamiltonian H and its a-Fermi maps write

$$\hat{\mathcal{L}}_0 = -4i \sum_{j,k} \hat{c}_j^\dagger H_{jk} \hat{c}_k, \quad (7)$$

the second part $\mathcal{L}_{diss} \rho := \mathcal{L}_{eff} + \kappa \mathcal{L}_{jump} = \sum_\mu (2\kappa L_\mu \rho L_\mu^\dagger - \rho L_\mu^\dagger L_\mu - L_\mu^\dagger L_\mu \rho)$ represents the dissipation, here we divided it into \mathcal{L}_{eff} and \mathcal{L}_{jump} , which is induced by the effective theory and jumping terms, respectively. It will allow us to quantify the effect of the quantum jump

$$\hat{\mathcal{L}}_{eff} = \sum_{j,k,\mu} 2l_{\mu,j} l_{\mu,k}^* (\hat{c}_j^\dagger \hat{c}_k^\dagger + \hat{c}_j \hat{c}_k), \quad (8)$$

$$\hat{\mathcal{L}}_{jump} = \sum_{j,k,\mu} 2l_{\mu,j} l_{\mu,k}^* e^{i\pi \hat{N}} (\hat{c}_j^\dagger \hat{c}_k^\dagger - \hat{c}_j^\dagger \hat{c}_k - \hat{c}_k^\dagger \hat{c}_j - \hat{c}_j \hat{c}_k), \quad (9)$$

where $\hat{N} = \sum_j \hat{c}_j^\dagger \hat{c}_j$ is the total number of ‘‘a-fermions’’, in the even parity subspace Eq. (9) becomes [35]

$$\hat{\mathcal{L}}_{jump} = \sum_{j,k,\mu} 2l_{\mu,j} l_{\mu,k}^* (\hat{c}_j^\dagger \hat{c}_k^\dagger - \hat{c}_j^\dagger \hat{c}_k - \hat{c}_k^\dagger \hat{c}_j - \hat{c}_j \hat{c}_k). \quad (10)$$

When considering the full dynamic ($\kappa = 1$), by using Eq. (8),(10), $\hat{\mathcal{L}}_{diss}$ writes

$$\hat{\mathcal{L}}_{diss} = \sum_{j,k,\mu} l_{\mu,j} l_{\mu,k}^* (4\hat{c}_j^\dagger \hat{c}_k^\dagger - 2\hat{c}_j^\dagger \hat{c}_k - 2\hat{c}_k^\dagger \hat{c}_j). \quad (11)$$

Together Eq. (7) and Eq. (11), and after reducing to normal master modes (NMMs), $\hat{a}_{2j-1} = 1/\sqrt{2}(\hat{c}_j + \hat{c}_j^\dagger)$, $\hat{a}_{2j} = i/\sqrt{2}(\hat{c}_j - \hat{c}_j^\dagger)$ [35], the Liouvillian can be written as

$$\hat{\mathcal{L}} = \sum_{j,k} \hat{a}_j \mathbf{A} \hat{a}_k, \quad (12)$$

where the \mathbf{A} is usually named as *shape matrix*, whose elements satisfy

$$\mathbf{A}_{2j-1,2k-1} = -2iH_{jk} - \sum_\mu l_{\mu,j} l_{\mu,k}^* + \sum_\mu l_{\mu,k} l_{\mu,j}^*, \quad (13a)$$

$$\mathbf{A}_{2j-1,2k} = -2H_{jk} + 2i \sum_\mu l_{\mu,k} l_{\mu,j}^*, \quad (13b)$$

$$\mathbf{A}_{2j,2k-1} = 2H_{jk} - 2i \sum_\mu l_{\mu,j} l_{\mu,k}^*, \quad (13c)$$

$$\mathbf{A}_{2j,2k} = -2iH_{jk} + \sum_\mu l_{\mu,j} l_{\mu,k}^* - \sum_\mu l_{\mu,k} l_{\mu,j}^*. \quad (13d)$$

The shape matrix of the model

By applying Eq. (7),(11) to our model (Fig.1(a)), the shape matrix \mathbf{A} could be split into \mathbf{A}_0 derived from the free Hamiltonian H part and \mathbf{A}_{diss} from the dissipation part

$$\mathbf{A}_0 = \begin{pmatrix} t_1 T & & & t_2 T \\ t_1 T & t_2 T & & \\ & t_2 T & t_1 T & \\ & & \ddots & \ddots \\ t_2 T & & & \end{pmatrix}, \quad (14)$$

here $T = -i\sigma_y \otimes I$, where σ_y is the pauli matrix and I is the identity operator. Here, for the sake of simplicity, we only consider the special case where there is only loss in the dissipation term \mathbf{A}_{diss} (the loss and gain case will be discussed afterwards)

$$\mathbf{A}_{diss} = \begin{pmatrix} A & B & & \\ -B & A & & \\ & A & B & \\ & & \ddots & \ddots \\ & & & -B & A \end{pmatrix}, \quad (15)$$

where the A and B can be calculated through Eq. (3a),(8),(9) with

$$A = -\frac{\gamma_l}{2} \begin{pmatrix} 0 & -i\kappa & -i & \kappa \\ i\kappa & 0 & \kappa & i \\ i & -\kappa & 0 & -i\kappa \\ -\kappa & -i & i\kappa & 0 \end{pmatrix}, B = -\frac{\gamma_l}{2} \begin{pmatrix} i & -\kappa & 0 & -i\kappa \\ -\kappa & -i & i\kappa & 0 \\ 0 & i\kappa & i & -\kappa \\ -i\kappa & 0 & -\kappa & -i \end{pmatrix}. \quad (16)$$

Suppose the model is under period boundary condition (PBC), it is relatively simple to transform into the momentum space, with the Fourier transform, the Bloch shape matrix writes

$$\tilde{\mathbf{A}}(k) = \begin{pmatrix} A & (t_1 + t_2 e^{-ik})T + B \\ (t_1 + t_2 e^{ik})T - B & A \end{pmatrix}. \quad (17)$$

On the other side, when the jumping terms are absent ($\kappa = 0$), the shape matrix $\mathbf{A}' = \mathbf{A}_0 + \mathbf{A}'_{diss}$ is now

$$\mathbf{A}' = -\frac{\gamma_l}{2} \begin{pmatrix} 0 & 0 & -i & 0 \\ 0 & 0 & 0 & i \\ i & 0 & 0 & 0 \\ 0 & -i & 0 & 0 \end{pmatrix}, B' = -\frac{\gamma_l}{2} \begin{pmatrix} i & 0 & 0 & 0 \\ 0 & -i & 0 & 0 \\ 0 & 0 & i & 0 \\ 0 & 0 & 0 & -i \end{pmatrix}. \quad (18)$$

Similarly by using Eq. (8),(9) the Bloch form shape matrix $\mathbf{A}'(k)$ is the same as Eq. (17), except that A, B is substituted by A', B'

$$\mathbf{A}'(k) = \begin{pmatrix} A' & (t_1 + t_2 e^{-ik})T + B' \\ (t_1 + t_2 e^{ik})T - B' & A' \end{pmatrix}. \quad (19)$$

Since for our system, the overall loss (correspond to the last term in Eq. (4)), A' can be neglected because the Liouvillian \mathcal{L} remains unchanged after a gauge shift $H \rightarrow H + cI$, where I is the identity operator and c is a complex c-number [38].

By using Eq. (14)-(19), we can find that \mathbf{A}, \mathbf{A}' have the same set of eigenvalues $\{\lambda\} = \sum_{\mu} E_{\mu}$ (where the eigenvalues with positive real parts are usually named as “rapidities” [35]. Here we use the label μ to represent different bands (or solutions))

$$\begin{aligned} E_{1,\pm}(\beta) &= \gamma/2 \pm \sqrt{(\gamma/2 + t_1 + t_2\beta)(\gamma/2 - t_1 - t_2\beta)}, \\ E_{2,\pm}(\beta) &= -\gamma/2 \pm \sqrt{(\gamma/2 + t_1 + t_2\beta)(\gamma/2 - t_1 - t_2\beta)}, \end{aligned} \quad (20)$$

regardless of the jump parameter κ , here we use the notation $e^{ik} = \beta$.

III. SYMMETRY

In the previous section, we introduce the model and demonstrate the shape matrix when the jumping terms are absent or presented. In order to know the property of a topological system, finding out its symmetry may be useful in determining its property. For the noninteracting fermions, it is proved that it can be sorted by the Altland-Zirnbauer (AZ) symmetry class [39–41], by judging the presence or absence of three basic symmetries, time-reversal symmetry (TRS), particle-hole symmetry (PHS), chiral symmetry (or sublattice symmetry), whose combinations will process a ten-fold classification

$$\text{TRS}: H = U_T H^* U_T^\dagger, U_T U_T^* = \pm I, \quad (21a)$$

$$\text{PHS}: H = -U_C H^* U_C^\dagger, U_C U_C^* = \pm I, \quad (21b)$$

$$\text{chiral}: H = -U_S H U_S^\dagger, U_S^2 = I, \quad (21c)$$

here U_T, U_C, U_S are all unitary matrices, corresponding to the TRS, PHS and chiral symmetry, respectively. When moving to open quantum systems, the quadratic Lindbladians still retain similar classifications [42, 43].

Precisely, by using pauli matrix, we can rewrite Eq. (17) as

$$\begin{aligned} \mathbf{A}(k) &= -i(t_1 + t_2 \cos k) \sigma_x \otimes (\sigma_y \otimes I_2) - it_2 \sin k \sigma_y \otimes \\ &(\sigma_y \otimes I_2) - \frac{i\gamma}{2} \sigma_y \otimes (I_2 \otimes (i\sigma_z - \kappa \sigma_x) + i\kappa \sigma_y \otimes \sigma_y) - \frac{\gamma}{2} \kappa I_2 \\ &\otimes I_2 \otimes \sigma_y + \frac{i\gamma}{2} I_2 \otimes \sigma_y \otimes (i\sigma_z - \kappa \sigma_x), \end{aligned} \quad (22)$$

when there is no jump and we neglect the overall loss, Eq. (19) becomes

$$\begin{aligned} \mathbf{A}'(k) &= -i(t_1 + t_2 \cos k) \sigma_x \otimes (\sigma_y \otimes I_2) - it_2 \sin k \sigma_y \otimes \\ &(\sigma_y \otimes I_2) + \frac{\gamma}{2} \sigma_y \otimes I_2 \otimes \sigma_z. \end{aligned} \quad (23)$$

Obviously, it is easy to prove that the Eq. (22) fulfills TRS in Eq. (21b), and $U_T U_T^* = -I$

$$U_T \mathbf{A}^*(k) U_T^{-1} = \mathbf{A}(-k), \quad (24)$$

and $U_T = I_2 \otimes \sigma_y \otimes \sigma_x$. While the Eq. (23) satisfies chiral symmetry in Eq. (21c)

$$\mathbf{A}'(k) = U_S \mathbf{A}'(k) U_S^{-1}, \quad (25)$$

and $S = \sigma_z \otimes I_2 \otimes I_2$, meanwhile $\mathbf{A}'(k)$ also has other symmetries (TRS in Eq. (21a) and PHS in Eq. (21b))

$$\mathbf{A}'(k) = U_T \mathbf{A}'(-k) U_T^{-1}, \quad (26)$$

$$\mathbf{A}'(k) = -U_C \mathbf{A}'(-k) U_C^{-1}, \quad (27)$$

where $U_T = I_2 \otimes \sigma_y \otimes \sigma_x$ and $U_C = \sigma_z \otimes \sigma_y \otimes \sigma_x$. By applying the classification method in Appendix A, the entire dynamic in Eq. (22) is of Class CII, and the jumping terms will break PHS and chiral symmetry, and yields an AII class.

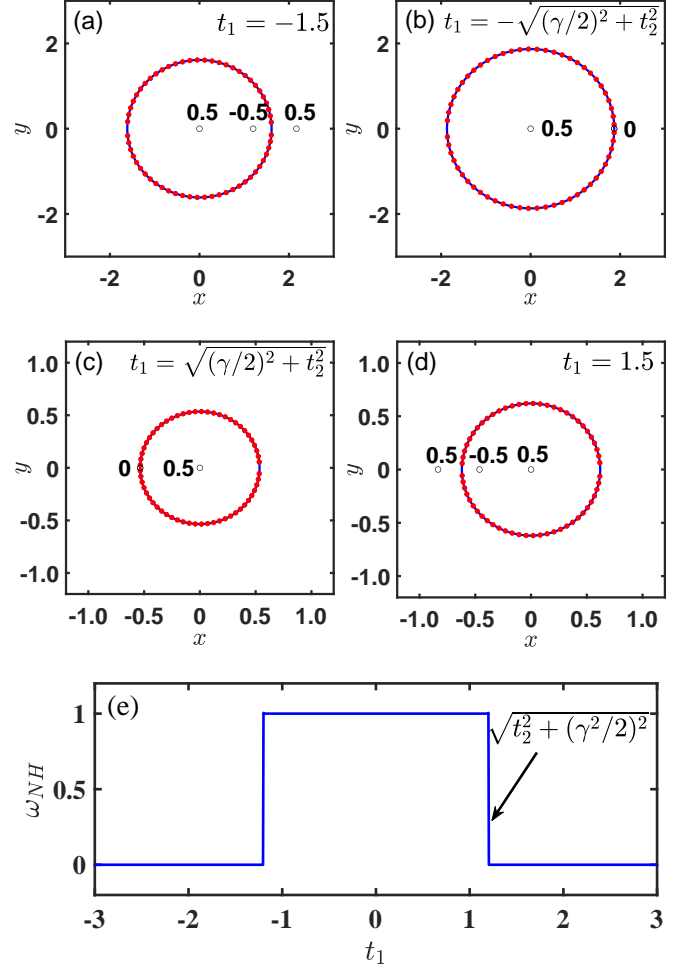


FIG. 2. (a-d) The GBZ of the effective Model (Fig. 1(b)), poles (black circles) and the corresponding residues of the winding number in Eq. (45). The blue solid lines represent the GBZ obtained by aGBZ theory, whereas the red points are the numerical results of Eq. (33) ($N = 60$). The parameters are chosen as (a) $t_1 = -1.5$, (b) $t_1 = \sqrt{(\gamma/2)^2 + t_2^2} \approx -1.2019$, (c) $t_1 = -\sqrt{(\gamma/2)^2 + t_2^2} \approx 1.2019$, (d) $t_1 = 1.5$. The 0 residues in (b),(c) are the second order poles, while others are of the first order. (e) The topological invariant as a function of t_1 , the transition points are at $t_1 = \pm \sqrt{(\gamma/2)^2 + t_2^2}$. In (a-e) we have $t_2 = 1, \gamma = 4/3$.

IV. GENERALIZED BRILLOUIN ZONE

The research of band theory is inextricably tied to the Brillouin zone. As a fundamental property in Hermitian topological systems, the bulk-edge correspondence has been extensively investigated. It reveals that the number of the edge states of the system under open boundary condition (OBC) can be predicted by topological invariant under PBC, and the definition and calculation of the invariant require the Brillouin zone. Nevertheless, the promotion to non-Hermitian systems is still a pending issue, even the simplest NH SSH models are controversially debated and discussed. Ref. [6] defines two half winding numbers around the exception points of a 2×2 Hamiltonian, each of which corresponds to an edge state, and implies that the conclusions held in Hermitian systems may fail in NH systems. In order to match these conclusions, Ref. [10] studies a non-Hermitian SSH model and defines a pair of fractional winding numbers with geometrical interpretation, and their summation determines the whole winding number of the entire system. However, it is argued by Ref. [2, 11] because this topological winding number defined in this manner fails to predict the appearance of the phase transition points. During recent years the relatively most accepted theory [2] proposes the concept of generalized Brillouin zone, they present that the momentum k in Hermitian cases is now complex in non-Hermitian systems, and instead, the phase factor in Bloch waves e^{ik} is replaced by β , whose real and imaginary parts in phase space is generally no longer a unit circle (see Appendix B for more details). Besides, in some NH systems, the wave function may not spread across the bulk, but localizes at the boundary (dubbed the “Non-Hermitian skin effect”) [44]. Though there are still some works that present a diverse range of opinions [9, 45], the theory of GBZ sparks a wave of researches on topological non-Hermitian systems [46–49].

Resultant

To obtain the information of the GBZ, the numerical solutions of the OBC spectrum shall be calculated first, which is the intrinsic requirement of the eigen-function. However, in practice the choice of the model dimension and calculation precision will tremendously affect the contours of GBZ, and the inappropriate value selection may cause unpredictable errors, or unacceptable calculation time. To avoid these problems, we use a kind of analytic calculation method introduced in Ref. [50], where the authors use a mathematical technique called *Resultant* to deal with these equations, suppose there are two polynomials $f(x) = a_n x^n + \dots + a_0 = \prod_{i=1}^n (x - \xi_i)$, $g(x) = b_m x^m + \dots + b_0 = \prod_{j=1}^m (x - \eta_j)$ which respect to x , their *Resultant* is defined as

$$R_x(f, g) = a_n^m b_m^n \prod_{i,j} (\xi_i - \eta_j). \quad (28)$$

In math, the *Resultant* can be used to eliminate variables in the polynomial, and obtain the polynomial which only relies

on other variables. Precisely, suppose there are two polynomials function $f(x, y), g(x, y) = 0$, where f, g is a function of both x and y , to fully remove the effect of x , and only remains the variable y , the relationship satisfies

$$R_x[f(x, y), g(x, y)] = 0, \quad (29)$$

this property can help us to obtain the generalized Brillouin zone of the system, and will be discussed later.

The calculation of aGBZ

From Appendix B, we have known that $f(\beta, E) = 0$ and there shall have at least a pair of solutions β which has the same norm $|\beta_M| = |\beta_{M+1}|$, thus we can assume $\beta_M = \beta_0$ and $\beta_{M+1} = \beta_0 e^{i\theta}$, where β_0 is a complex number, so there will be

$$f(\beta_0, E) = f(\beta_0 e^{i\theta}, E) = 0, \theta \in \mathcal{R}. \quad (30)$$

By using the property of *Resultant* in Eq. (29), it is easy to eliminate E in Eq. (30), and yields

$$G(\beta, \theta) = R_E(f(\beta, E), f(\beta e^{i\theta}, E)) = 0. \quad (31)$$

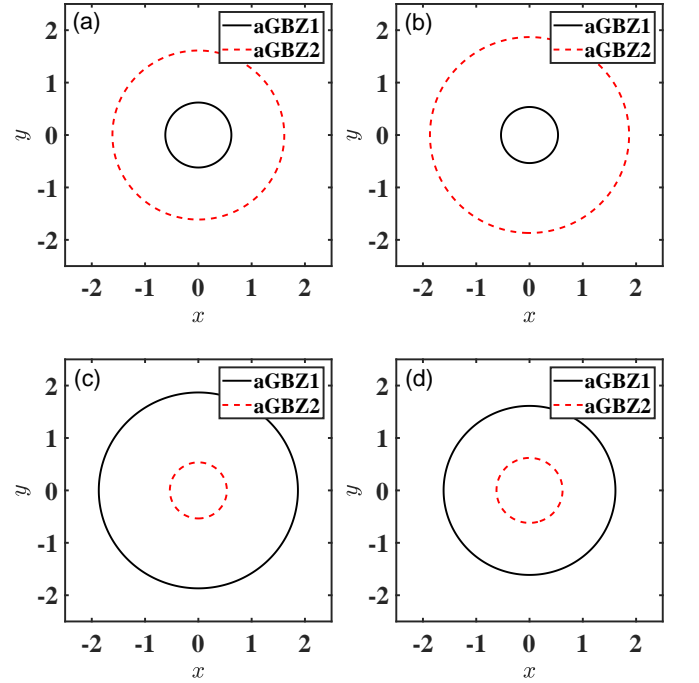


FIG. 3. The aGBZ of open quantum description (Eq. (19)) without quantum jump. The black solid and red dashed line are arcs of aGBZ in Eq. (37b)(38a). The same as Fig. 2(a)–2(d), parameters are chosen as (a) $t_1 = -1.5$, (b) $t_1 = -\sqrt{(\gamma/2)^2 + t_2^2}$, (c) $t_1 = \sqrt{(\gamma/2)^2 + t_2^2}$, (d) $t_1 = 1.5$, and $t_2 = 1, \gamma = 4/3$.

Obviously it requires both real and imaginary parts of $G(\beta, \theta)$ to be zero, $\text{Re}[G(\beta, \theta)] = 0, \text{Im}[G(\beta, \theta)] = 0$. The next step is to eliminate the variable θ , by using Weierstrass

substitution, $\cos \theta = (1 - t^2)/(1 + t^2)$, $\sin \theta = 2t/(1 + t^2)$, to substitute the parameter θ , and we have

$$R_t[Re(G(\beta, \theta)), Im(G(\beta, \theta))] = 0. \quad (32)$$

After the above treatments, both the variables E and θ will not appear anymore. And several nontrivial real constraint equations can be decomposed from Eq. (32), which outline the curves of auxiliary generalized Brillouin zone (aGBZ). In general, the actual GBZ is usually a subset of aGBZ [50].

The GBZ of the effective NH Hamiltonian

In this section, we first consider the GBZ of the effective non-Hermitian Eq. (4), and for the sake of simplicity, we consider $\gamma_g = 0$ and $\gamma_l = \gamma$ for short in Eq. (3a)(3b), and the model will be simplified to the case discussed in Ref. [2]

$$\left[\left(t_1 - \frac{\gamma}{2} \right) + t_2 \beta \right] \left[\left(t_1 + \frac{\gamma}{2} \right) + t_2 \beta^{-1} \right] = E^2, \quad (33)$$

here E is the energy of bulk-band in OBC, and the β is obtained by using Eq. (B7). By using the technique above, we substitute Eq. (33) into Eq. (31) and (32), and obtain the con-

straint equations of GBZ

$$\frac{\gamma}{2} - t_1 + \left(\frac{\gamma}{2} + t_1 \right) (x^2 + y^2) = 0, \quad (34a)$$

$$-\frac{\gamma}{2} + t_1 + \left(\frac{\gamma}{2} + t_1 \right) (x^2 + y^2) = 0, \quad (34b)$$

here $x = \text{Re}\beta$ and $y = \text{Im}\beta$, which describe the trajectory of β . In Fig. 2(a)-2(d) we display the GBZ of the effective model, calculated by methods of aGBZ (blue solid line). The scattered red dots are solved by numerical method (Eq. (33)), apparently the results are consistent, except that the trajectory comes extremely loose near the real axis, where the aGBZ solution gives an explicit closed region. Although the former is simpler to compute programmatically, the aGBZ scheme is more recommended to use.

The aGBZ of shape matrix when no jump

Next we calculate the GBZ of the shape matrix in open quantum description, we first consider when there is no jump (Eq. (19), and the overall loss is neglected), the dynamic is the same as the effective non-Hermitian (Eq. (4)). By using Eq. (B2), the eigen-function of \mathbf{A} at the bulk writes

$$\begin{pmatrix} 0 & 0 & -t_2 & 0 & 0 & 0 & 0 & 0 & -\frac{i\gamma}{2} & 0 & -t_1 & 0 & 0 & 0 & 0 & 0 \\ 0 & 0 & 0 & -t_2 & 0 & 0 & 0 & 0 & 0 & \frac{i\gamma}{2} & 0 & -t_1 & 0 & 0 & 0 & 0 \\ t_2 & 0 & 0 & 0 & 0 & 0 & 0 & 0 & t_1 & 0 & -\frac{i\gamma}{2} & 0 & 0 & 0 & 0 & 0 \\ 0 & t_2 & 0 & 0 & 0 & 0 & 0 & 0 & 0 & t_1 & 0 & \frac{i\gamma}{2} & 0 & 0 & 0 & 0 \\ 0 & 0 & 0 & 0 & \frac{i\gamma}{2} & 0 & -t_1 & 0 & 0 & 0 & 0 & 0 & 0 & 0 & -t_2 & 0 \\ 0 & 0 & 0 & 0 & 0 & -\frac{i\gamma}{2} & 0 & -t_1 & 0 & 0 & 0 & 0 & 0 & 0 & 0 & -t_2 \\ 0 & 0 & 0 & 0 & t_1 & 0 & \frac{i\gamma}{2} & 0 & 0 & 0 & 0 & 0 & t_2 & 0 & 0 & 0 \\ 0 & 0 & 0 & 0 & 0 & 0 & t_1 & 0 & -\frac{i\gamma}{2} & 0 & 0 & 0 & 0 & 0 & t_2 & 0 \end{pmatrix} \begin{pmatrix} \psi_{nA1} \\ \psi_{nA2} \\ \psi_{nA3} \\ \psi_{nA4} \\ \psi_{nB1} \\ \psi_{nB2} \\ \psi_{nB3} \\ \psi_{nB4} \\ \psi_{n+1A1} \\ \psi_{n+1A2} \\ \psi_{n+1A3} \\ \psi_{n+1A4} \\ \psi_{n+1B1} \\ \psi_{n+1B2} \\ \psi_{n+1B3} \\ \psi_{n+1B4} \end{pmatrix} = E \begin{pmatrix} \psi_{nA1} \\ \psi_{nA2} \\ \psi_{nA3} \\ \psi_{nA4} \\ \psi_{nB1} \\ \psi_{nB2} \\ \psi_{nB3} \\ \psi_{nB4} \end{pmatrix}, \quad (35)$$

where the eigenvectors of the shape matrix can be written as $|\Psi\rangle = (\psi_{1A1}, \psi_{1A2}, \psi_{1A3}, \psi_{1A4}, \psi_{1B1}, \psi_{1B2}, \psi_{1B3}, \psi_{1B4}, \dots)^T$, where $\psi_{m\sigma n}$ is the wave function at site $\sigma = A, B$, and m is the index of the cell, $n = 1, 2, 3, 4$ stands for the NMMs in Eq. (5).

After using the characteristic equation in Eq. (B3),(B4), in order to have non-zero solutions, the determinant of the

coefficient matrix shall equal to zero, it indicates

$$E^2 - \gamma^2/4 + t_1^2 + \frac{\gamma t_2}{2\beta} - \frac{\beta \gamma t_2}{2} + \frac{t_1 t_2}{\beta} + \beta t_1 t_2 + t_2^2 = 0, \quad (36a)$$

$$E^2 - \gamma^2/4 + t_1^2 - \frac{\gamma t_2}{2\beta} + \frac{\beta \gamma t_2}{2} + \frac{t_1 t_2}{\beta} + \beta t_1 t_2 + t_2^2 = 0, \quad (36b)$$

by substituting Eq. (36a),(36b) into Eq. (31),(32) to eliminate the addition degrees E, θ , the irreducible factors of $R_t[Re(G), Im(G)] = 0$ presents the trajectory of aGBZ. Eq.

(36a) indicates

$$-\gamma/2 - t_1 + (\gamma/2 - t_1)(x^2 + y^2) = 0, \quad (37a)$$

$$\text{or } \gamma/2 + t_1 + (\gamma/2 - t_1)(x^2 + y^2) = 0, \quad (37b)$$

while Eq. (36b) shows

$$\gamma/2 - t_1 + (\gamma/2 + t_1)(x^2 + y^2) = 0, \quad (38a)$$

$$\text{or } -\gamma/2 + t_1 + (\gamma/2 + t_1)(x^2 + y^2) = 0, \quad (38b)$$

same as the previous, x, y takes $x = \text{Re}\beta$ and $y = \text{Im}\beta$.

The Eq. (37a)-(38b) actually correspond to two separate closed regions for a set of given parameters, in Fig. 3(a)-3(d) we show the curves of aGBZ plotted under several sets of parameters. Here we shall stress that when using the aGBZ method to calculate GBZ, incremental solutions are usually introduced, because the actual spectrum of OBC has a bounded range of values, however, we eliminate E in Eq. (31), which means all possible values of E in the complex plane can be taken, thus an inspection is required. Nevertheless, for particular circumstances, the model may have multi GBZ bands, the most common case is that different decompositions $E_\mu(\beta)$ of the characteristic equation in Eq. (B4) may lead to distinct sub-GBZ bands (Eq. (B5)). In Appendix C, we briefly

introduce the definition of self-conjugate points in aGBZ, and any analytic arc that contains these points must form the GBZ, which allows us to accurately determine the actual area of the GBZ.

As an example, in Fig. 4(a)-4(d), we show the end points E_0 of the spectrum (red points) by solving Eq. (C4) when $t_1 = \sqrt{(\gamma/2)^2 + t_2^2} \pm 0.05$, which is close to the transition points. By using the procedures above, we mark the corresponding β_0 in Fig. 4(a),4(b) with cyan squares, that pass through the curves of both aGBZ, by applying the previous conclusions, both branches of the closed loop in Fig. 3(a)-3(d) are either aGBZ or GBZ.

The GBZ of shape matrix when jump presented

In order to visualize the effect of jumping terms, in this subsection, we use the above methods for the case that quantum jumps are included. In other words, the dynamic of the master equation introduced in Eq. (1), by substituting Eq. (14)(15) into Eq. (B3), the eigen-function will become

$$\begin{pmatrix} \frac{i\gamma}{2} & -\frac{\gamma}{2}\kappa & -t_1 & -\frac{i\gamma}{2}\kappa & 0 & \frac{i\gamma}{2}\kappa & \frac{i\gamma}{2} & -\frac{\gamma}{2}\kappa & 0 & 0 & -t_2 & 0 & 0 & 0 & 0 & 0 \\ -\frac{\gamma}{2}\kappa & -\frac{i\gamma}{2} & \frac{i\gamma}{2}\kappa & -t_1 & -\frac{i\gamma}{2}\kappa & 0 & -\frac{\gamma}{2}\kappa & -\frac{i\gamma}{2} & 0 & 0 & 0 & -t_1 & 0 & 0 & 0 & 0 \\ t_1 & \frac{i\gamma}{2}\kappa & \frac{i\gamma}{2} & -\frac{\gamma}{2}\kappa & -\frac{i\gamma}{2}\kappa & \frac{\gamma}{2}\kappa & 0 & \frac{i\gamma}{2}\kappa & t_2 & 0 & 0 & 0 & 0 & 0 & 0 & 0 \\ -\frac{i\gamma}{2}\kappa & t_1 & -\frac{\gamma}{2}\kappa & -\frac{i\gamma}{2} & \frac{\gamma}{2}\kappa & \frac{i\gamma}{2} & -\frac{i\gamma}{2}\kappa & 0 & 0 & t_2 & 0 & 0 & 0 & 0 & 0 & 0 \\ 0 & 0 & 0 & 0 & 0 & 0 & -t_2 & 0 & 0 & \frac{i\gamma}{2}\kappa & \frac{i\gamma}{2} & -\frac{\gamma}{2}\kappa & -\frac{i\gamma}{2} & \frac{\gamma}{2}\kappa & -t_1 & \frac{i\gamma}{2}\kappa \\ 0 & 0 & 0 & 0 & 0 & 0 & 0 & -t_2 & -\frac{i\gamma}{2}\kappa & 0 & -\frac{\gamma}{2}\kappa & -\frac{i\gamma}{2} & \frac{\gamma}{2}\kappa & -\frac{i\gamma}{2} & -t_1 & -\frac{i\gamma}{2}\kappa \\ 0 & 0 & 0 & 0 & t_2 & 0 & 0 & 0 & -\frac{i\gamma}{2} & \frac{\gamma}{2}\kappa & 0 & \frac{i\gamma}{2}\kappa & t_1 & -\frac{\gamma}{2}\kappa & -\frac{i\gamma}{2} & \frac{\gamma}{2}\kappa \\ 0 & 0 & 0 & 0 & 0 & t_2 & 0 & 0 & \frac{\gamma}{2}\kappa & \frac{i\gamma}{2} & -\frac{i\gamma}{2}\kappa & 0 & \frac{i\gamma}{2}\kappa & t_1 & \frac{\gamma}{2}\kappa & \frac{i\gamma}{2} \end{pmatrix} \begin{pmatrix} \psi_{nA1} \\ \psi_{nA2} \\ \psi_{nA3} \\ \psi_{nA4} \\ \psi_{nB1} \\ \psi_{nB2} \\ \psi_{nB3} \\ \psi_{nB4} \\ \psi_{n+1A1} \\ \psi_{n+1A2} \\ \psi_{n+1A3} \\ \psi_{n+1A4} \\ \psi_{n+1B1} \\ \psi_{n+1B2} \\ \psi_{n+1B3} \\ \psi_{n+1B4} \end{pmatrix} = E \begin{pmatrix} \psi_{nA1} \\ \psi_{nA2} \\ \psi_{nA3} \\ \psi_{nA4} \\ \psi_{nB1} \\ \psi_{nB2} \\ \psi_{nB3} \\ \psi_{nB4} \end{pmatrix}, \quad (39)$$

following similar procedures, we will have

$$E^2 - \gamma E + \frac{\gamma t_2}{2\beta} - \frac{\gamma t_2}{2}\beta + \frac{t_1 t_2}{\beta} + \beta t_1 t_2 + t_1^2 + t_2^2 = 0, \quad (40a)$$

$$E^2 + \gamma E - \frac{\gamma t_2}{2\beta} + \frac{\gamma t_2}{2}\beta + \frac{t_1 t_2}{\beta} + \beta t_1 t_2 + t_1^2 + t_2^2 = 0, \quad (40b)$$

which is independent of the jumping strength κ . When $\kappa = 0$ and the overall loss is neglected, we will return to the no jump case (Eq. (35)). By performing the same procedures in the previous subsection, we will find Eq. (40a) and Eq. (40b) lead to the same GBZ region in Eq. (37a)-Eq. (38b).

V. TOPOLOGICAL INVARIANTS WITH OR WITHOUT QUANTUM JUMP

The interest in research of non-Hermitian topological invariant is rising and remarkable progress has been made in recent years. However, the studies of the corresponding extension to open quantum systems are not particularly abundant. For instance, Ref. [27] compares the zak phase defined by using the biorthogonal basis of the effective PT (spatial inversion and time reflection) non-Hermitian Hamiltonian as well as the shape matrix after the third quantization, the former one has

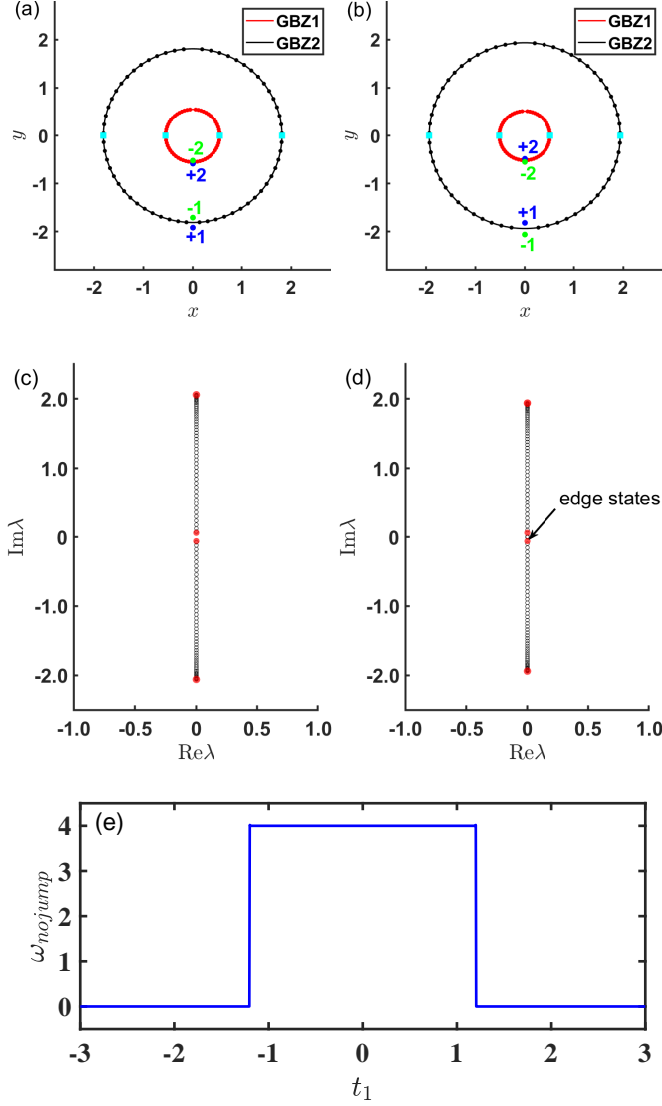


FIG. 4. (a-b) The GBZ of jumping absent shape matrix \mathbf{A}' , the red and black solid line is for the arc of GBZ1 and GBZ2 respectively, the scattered dots are the numerical result by solving Eq. (36b)(36b) with $N = 60$. The cyan squares represent the self-conjugate points ($\beta_M = \beta_{M+1}$), the blue and green points are the zeros of $\det(h_1)$ and $\det(h_2)$. (c-d) The spectrum of \mathbf{A}' close to the transition point (black circles, $N = 50$). In (a,c) $t_1 = \sqrt{(\gamma/2)^2 + t_2^2} + 0.05 \approx 1.2519$, and in (b,d) $t_1 = \sqrt{(\gamma/2)^2 + t_2^2} - 0.05 \approx 1.1519$. $t_2 = 1, \gamma = 4/3$. The red dots represent the self-conjugate points, which restrict the range of the energy spectrum under OBC. It is clear that there is zero eigen-energy in (d) (eightfold degenerate). (e) The winding number calculated by Eq. (47), when there is no quantum jump.

only stable region when PT-symmetric is unbroken, while the latter has two dissipation strength independent regions which each holds a stable zak phase 0 or π , inherits from Hermitian cases. Ref. [26] studies the concept of topological order in open fermion systems by focusing on a different paradigm, that is, the density matrix of the system. In this manner, sev-

eral illustrative examples such as Bardeen–Cooper–Schrieffer (BCS) model are given out, and their symmetry class and winding number are also analyzed. Besides, the definition of winding number in NH systems also has multiple opinions, such as in Ref. [51], the phase diagram of a SSH model with intra-sublattice dissipation is given forth by using the NH symmetry classification. In contrast, in Ref. [2], the types of the invariants are inherited from the Hermitian symmetry classification, except that the integral path is replaced by GBZ from the conventional BZ. We must emphasize that these existing studies are to some extent an exploration or extension based on existing topological theories.

Back to our model, since the GBZ region and symmetry classification of our model are clear in Sec. III, IV, we can now consider the definition of their topological invariants by combining the open quantum description and the GBZ method together.

In Sec. III, we have known that when there is no jump, the shape matrix \mathbf{A}' (Eq. (19)) follows chiral symmetry, and the invariants corresponding to this symmetry is usually defined by the “Q” matrix approach [52]. By choosing a proper basis that makes the symmetry operator diagonal, the Hamiltonian H can also be written as

$$H = \begin{pmatrix} h_+ & \\ & h_- \end{pmatrix}, \quad (41)$$

where h_{\pm} is a matrix and for Hermitian cases $h_- = h_+^*$. For a non-Hermitian system, the special internal symmetry may determine a relationship between h_+ and h_- [32]. The eigenvectors and eigenvalues of H satisfy [13]

$$h_+ h_- |\psi_{\mu}^R\rangle = E_{\mu}^2(\beta) |\psi_{\mu}^R\rangle, \quad (42)$$

where the $\{|\psi_{\mu}^R\rangle\}, \{|\psi_{\mu}^L\rangle\}$ is the set of right and left eigenvectors and $\langle\psi_{\nu}^L|\psi_{\mu}^R\rangle = \delta_{\mu,\nu}$. Hence the Q matrix can be calculated

$$Q = \begin{pmatrix} q(\beta) \\ q^{-1}(\beta) \end{pmatrix}, \quad (43)$$

where $q(\beta) = \sum_{\mu} q_{\mu}(\beta) = \sum_{\mu} \frac{1}{E_{\mu}(\beta)} |\psi_{R,\mu}(\beta)\rangle \langle\psi_{L,\mu}(\beta)| h_+$, the $q_{\mu}(\beta)$ corresponds to different band $E_{\mu}(\beta)$, respectively. The total winding number can be defined via the Q matrix, for instance in a 1D system with only one region of GBZ [53],

$$\omega_{\mu} = \frac{1}{2\pi i} \oint_{\beta_{GBZ}} \text{Tr}[q(\beta)^{-1} dq(\beta)] = \frac{1}{2\pi i} \oint_{\beta_{GBZ}} d \ln \det[q(\beta)], \quad (44)$$

where the β_{GBZ} is the GBZ of the model.

For the effective Hamiltonian we consider in Eq. (4), according to Eq. (44), it is easy to know that $h_+ = t_1 + t_2/\beta + \gamma/2$, $h_- = t_1 + t_2\beta - \gamma/2$, and the total winding number is defined as

$$\omega_{NH} = \frac{1}{2\pi i} \oint_{\beta_{NH}} \left(\frac{t_2}{2\beta(\gamma/2 + t_1) + t_2} - \frac{t_2}{2(\gamma/2 - (t_1 + \beta t_2))} \right) d\beta, \quad (45)$$

the GBZ region β_{NH} is depicted by Eq. (34a)(34b). In Fig. 2(e), we plot the chiral winding number calculated by Eq. (45) as a function of t_1 .

Next, we will turn to the open quantum system, from Eq. (22), similarly we have

$$\begin{aligned} h_+ &= -i(t_1 + t_2 \cos k)(\sigma_y \otimes I_2) - t_2 \sin k(\sigma_y \otimes I_2) - i\gamma I_2 \otimes \sigma_z, \\ h_- &= -i(t_1 + t_2 \cos k)(\sigma_y \otimes I_2) + t_2 \sin k(\sigma_y \otimes I_2) + i\gamma I_2 \otimes \sigma_z. \end{aligned} \quad (46)$$

In this case, calculating the winding number of the system will be a bit complicated, since we will face the problem of integration over multiple GBZ. Based on intuition, we shall combine Eq. (41),(44),(46), and write the total winding number as a sum of all GBZ bands $\beta_{GBZ,\mu}$

$$\omega_{no\ jump} = \frac{1}{2\pi i} \sum_{\mu} \oint_{\beta_{GBZ,\mu}} \text{Tr} [q_{\mu}^{-1} \partial_{\beta} q_{\mu}]. \quad (47)$$

As Sec. IV and Appendix C show, the region of $\beta_{GBZ,1,2}$ is given by Eq. (37a)- Eq. (38b). However, this is not the case in reality, because the sum of the winding number of each band $E_{\mu}(\beta)$ in Eq. (47), we will have

$$\sum_{\mu} \text{Tr}(q_{\mu}^{-1} dq_{\mu}) = \sum_{\mu} d \ln \det(q_{\mu}) \neq d \ln \det(\sum_{\mu} q_{\mu}). \quad (48)$$

Thus supposing $\beta_{GBZ,1}$ coincides with $\beta_{GBZ,2}$, Eq. (47) cannot be reduced to the previous single GBZ cases as Eq. (44). Here we use the “wave function” method introduced in [50], which is

$$\omega_{no\ jump} = \frac{1}{2}(\omega_+ - \omega_-), \quad \omega_{\pm} = -P_{\pm} + \sum_{\mu} Z_{\pm,\mu}, \quad (49)$$

where P_{\pm} is the order of the pole of $\det(h_{\pm})$, and $Z_{\pm,\mu}$ is the number of the zeros that not only satisfy $\det(h_{\pm}(\beta)) = E_{\mu}(\beta)$, but also inside its corresponding sub-GBZ $_{\mu}$. The basic idea of this equation is a promotion of the multi-band winding number, and the proof of this formula requires *Cauchy's argument principle* [54]. When the zeros that do not belong to the band $E_{\mu}(\beta)$ pass through the corresponding GBZ $_{\mu}$, they will not contribute to the winding number. By using Eq. (46), $\det(h_+) = (\gamma^2 - 4(t_1 - it_2\beta)^2)/16$, $\det(h_-) = (\beta^2(\gamma^2 - 4t_1^2) - 8i\beta t_1 t_2 + 4t_2^2)/(16\beta^4)$, it is worth stressing that the zeros are all double degenerate, and we can also find $P_+ = 0, P_- = 4$. In Fig. 4(a),4(b) we denote all the zeros Z_{\pm} with blue and green dots. In Fig. 4(a), from the definition of Z_{\pm} , it is easy to find that the zeros ± 2 belong to GBZ $_1$ while ± 1 belong to GBZ $_2$. Since the zero $+1, +2$ is outside GBZ $_{2,1}$, they do not contribute to the total winding number, which means $Z_{+1,2} = 0$. Meanwhile, because of degeneracy, the zeros $-1, -2$ each correspond to $Z_{-2,1} = 2$, thus we have $\omega_{no\ jump} = 0$. Similarly, in Fig. 4(b), $Z_{+1,2} = 2, Z_{-1,-2} = 0$, and the total winding number $\omega_{no\ jump} = 4$. By using this technique, we can calculate the invariant that changes with t_1 in Fig. 4(e) by using Eq. (49).

After the above analysis, an important property is that the topological invariants in open quantum description can predict the transition points as in NH systems. For example, from

Fig. 2(b), 2(c) for the effective NH system and Fig. 3(b),3(c) for the jump absent open system description, although the dimensions and used methods are totally different, the transition points appear at the same location. It proves the validity of our scheme in describing the phases of open systems, and may also help us to study the nature of the system when quantum jumps are involved.

In Sec. III, we have learned that when jumping terms are presented, the shape matrix \mathbf{A} is time-reversal symmetric, which means its Bloch form obeys relation $\mathbf{A}(-k) = U_T \mathbf{A}^*(k) U_T^\dagger$, and $U_T = I_2 \otimes \sigma_y \otimes \sigma_x$ is unitary and Hermitian, thus we can choose $\mathcal{P} = U_T$ and $\mathcal{T} = \mathcal{K}$, where \mathcal{K} is conjugation operator, hence $\mathbf{A}(k)\mathcal{P}\mathcal{T} = \mathcal{P}\mathcal{T}\mathbf{A}(k)$. In other word, the shape matrix is $\mathcal{P}\mathcal{T}$ invariant under combined action of parity

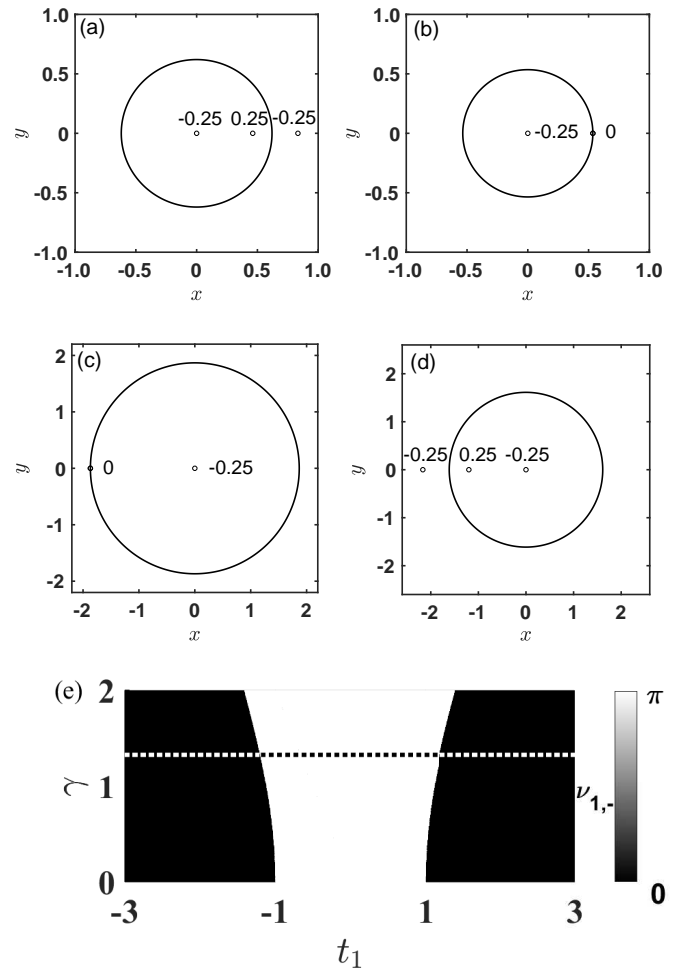


FIG. 5. (a-d) The GBZ of band $E_{1,-}$ when jumping terms are included. To show the differences and similarities, parameters are chosen as the same as in Fig. 3(a)-3(d). The number is the residue of the corresponding pole of zak phase $\nu_{1,-}$. The 0 residue in (b)(c) is the second order pole, while others are of the first order. (e) The phase diagram of zak phase $\nu_{1,-}$ respect with t_1 and γ , where κ takes 1. The black region corresponds to a 0 zak phase and the white region represents a π zak phase. The dashed line represents the previous set of parameters when $\gamma = 4/3$.

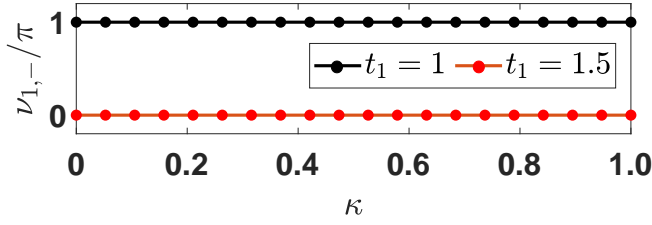


FIG. 6. The numerical result of the zak phase $\nu_{1,-}$ by using Eq. (50), corresponding to $E_{1,-}$ band, which respects to different jump parameter κ , we choose $t_2 = 1, \gamma = 4/3$. The black line and dots represent $t_1 = 1$ case, while the red line and dots represent $t_1 = 1.5$. The zak phase is unchanged under different values of κ .

and time inversion, $[\mathbf{A}, \mathcal{PT}] = 0$.

The zak phase in 1D system [55] is the analogue of the Berry phase that the particle picks up when moving across the Brillouin zone. When the Hamiltonian has PT symmetry, it is proved by Hatsugai *et al.* that the zak phase takes integer multiples of π [56]. Furthermore, with the introduction of the biorthogonal basis [57], the concept of the zak phase is gradually extended to non-Hermitian systems [58]. After the analysis above, we can define the zak phase of a given band as

$$\nu_\mu = i \oint_{\beta_{GBZ}} \langle l_\mu | \partial_\beta | r_\mu \rangle d\beta, \quad (50)$$

where β_{GBZ} is the GBZ of the selected band, the derivation of β is an extension of Hermitian cases, the $|l_\mu\rangle$ and $|r_\mu\rangle$ are the left and right eigenvectors of \mathbf{A} , associated with the band E_μ (Eq. (20)).

As an example, in Fig. 5(a)-5(d), we plot the GBZ of the band $E_{1,-}$ when jump is presented ($\kappa = 1$). The parameters are chosen as the same in the previous subsection. By using Eq. (50), we can obtain the analytical zak phase of $E_{1,-}$ band

$$\nu_{1,-} = i \oint_{\beta_{GBZ_{E_{1,-}}}} \frac{t_2(2\beta^2(t_1 - \gamma/2) + 4\beta t_2 + 2t_1 + \gamma)}{2\beta(\beta(\gamma - 2t_1) - 2t_2)(\gamma + 2(t_1 + \beta t_2))}, \quad (51)$$

where $\beta_{GBZ_{E_{1,-}}}$ is the loop restricted by Eq. (37a)(37b), by combing the two equations Eq. (20) and Eq. B4, corresponding to the band $E_{1,-}$. In this way, the zak phases for all the bands can be calculated.

In Fig. 5(e), we display the phase diagram describing the dependence of zak phase $\nu_{1,-}$ on t_1 and γ , where the black and white region contributes a 0 or π phase respectively. We can find that in the full area the zak phase is quantized, which is in contrast to previous studies, that it only appears in PT-unbroken regimes [59, 60]. The transition points are $t_1 = \pm \sqrt{(\gamma/2)^2 + t_2^2}$, and the dashed line stands for $\gamma = 4/3$ in Fig. 5(a)-5(d).

Finally, in order to visualize the effect of quantum jump events, in Fig. 6 we numerically calculate $\nu_{1,-}$ in various parameters of κ and t_1 . Intriguingly, it indicates that in this model, the jump does not influence the discussion above, the model has a κ independent zak phase. It seems that the quantum jump would not affect the winding number of the open

quantum system. However, it is a model-dependent issue. For the sake of simplicity, previously we only considered loss in Fig. 1(a), which leads to the fact that when writing the Liouvillian operator in the matrix representation (Fock space), the jumping terms $\kappa \mathcal{L}_{jump}$ link the subspaces of (N_0, N_0-1) , where N_0 is the total number of excited fermions; the other parts $\mathcal{L}_{without jump} = \mathcal{L}_0 + \mathcal{L}_{eff}$, conserve the number of particles, which link the subspaces of (N_0, N_0) . Mathematically, the jump absence terms can be written as block-diagonal forms, and the jumping terms are the block-upper-triangular terms, and the latter terms do not affect the Liouvillian spectrum $\{\Lambda\}$, regardless of PBC or OBC [17, 23]. In Fig. 7 we plot the full Liouvillian spectrum $\mathcal{L}_{full} = \mathcal{L}_{no jump} + \kappa \mathcal{L}_{jump}$ (red circles) and $\mathcal{L}_{no jump}$ (black dots), and their spectra show no difference, which proves our conjecture.

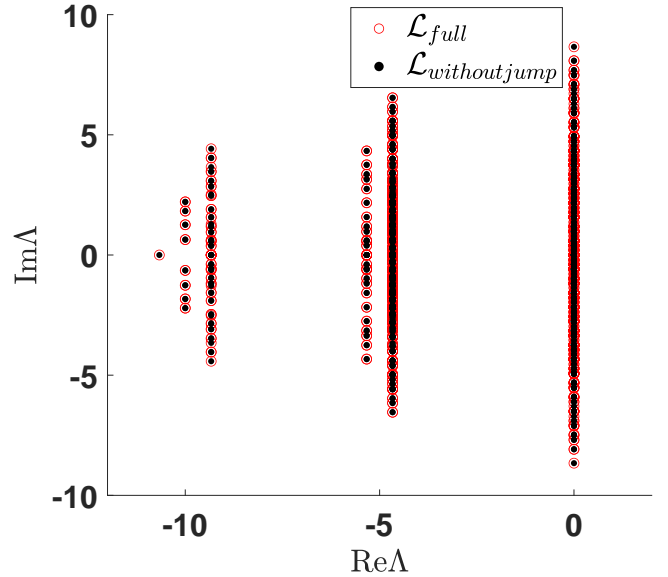


FIG. 7. Numerical result of the Liouvillian spectrum $\{\Lambda\}$ of our model, the calculation is based on the exact diagonalization method in Ref. [61]. The red circles represent the \mathcal{L}_{full} and the black dots are for $\mathcal{L}_{without jump}$. We restrict the subspaces of the maximum excitation is 2, $t_1 = 1.5, t_2 = 1, \gamma = 4/3, \kappa = 1, N = 8$.

Besides, it also means their rapidities of the shape matrix are all the same (actually, for PBC, we have already shown that they are the same, as in Eq. (20)), because the Liouvillian spectrum is a linear combination of the rapidities [35]. According to the characteristic equation (40a)(40b), the same spectrum induces the same region of GBZ, which does not depend on the change of κ .

For a more visual demonstration of the unique effects of quantum jumps, we show a circumstance that the GBZ is dependent on jump strength κ , when the Lindblad operators we considered in Eq. (3a),(3b) have both loss and gain, since the presence of gain in the system is essential to achieve a non-trivial nonequilibrium steady state (NESS) [33]. In this case, the jumping terms cannot be written as a matrix representation like the upper triangular block as before, which may indicate that they are non-negligible.

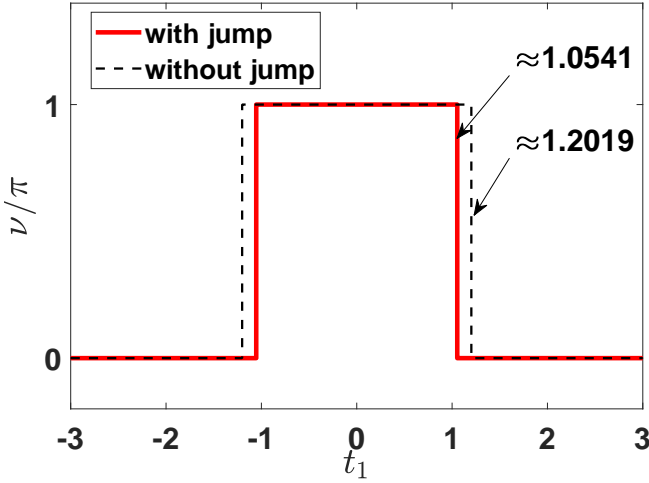


FIG. 8. The zak phase ν of a selected band when the system is suffering both loss and gain ($\kappa = 1$, red solid line), and the jumping absence case ($\kappa = 0$, black dashed line, as discussed in the main text), changes with t_1 . The transition points changed, which indicates that the jumping terms can not be safely neglected. Parameters are chosen as $t_2 = 1$, $\gamma_l = 1$, $\gamma_g = 1/3$.

By similar procedures in the main text, and consider $\kappa = 1$, their sub-GBZs are still circles, whose radius r are

$$r = \left| \frac{\gamma_l/2 - \gamma_g/2 + t_1}{\gamma_l/2 - \gamma_g/2 - t_1} \right|^{\pm \frac{1}{2}}. \quad (52)$$

It can be seen that the difference of the loss and gain rate $\gamma_l - \gamma_g$ may affect the region of GBZ, though in the effective theory their sum $\gamma_l + \gamma_g$ contributes to the non-reciprocal terms in Eq. (4). Moreover, when κ takes other values, the GBZ may no longer be a circle. In these cases, the jumping terms can not be safely neglected, which is different from the circumstance when there is only loss. In Fig. 8, we display the zak phase for the case when the system has both gain and loss (red solid line), and we also plot the result when the jumping terms are completely neglected (the black dashed line) as a comparison. The transition points are at $\pm \sqrt{t_2^2 + ((\gamma_l - \gamma_g)/2)^2}$, which is different from the no jumping case, and also demonstrates the necessity of our scheme.

To summarize, the effect of quantum jumping events in the system needs to be carefully examined and may significantly affect the conclusions in effective NH systems, our scheme can help to solve this problem to some extent.

Bulk-edge correspondence

In this subsection, we will show that the bulk-edge correspondence still holds in our scheme by examining the edge states of the shape matrix \mathbf{A} and \mathbf{A}' . Here as previous only the dissipation with loss is considered for simplicity. We mainly talk about \mathbf{A}' as an example in Fig. 9(a)-9(b), by numerically calculating the eigenvalues $\{\lambda\}$ of the shape matrix \mathbf{A}' under different parameters of t_1 . In Fig. 4(d), 9(b) it can be

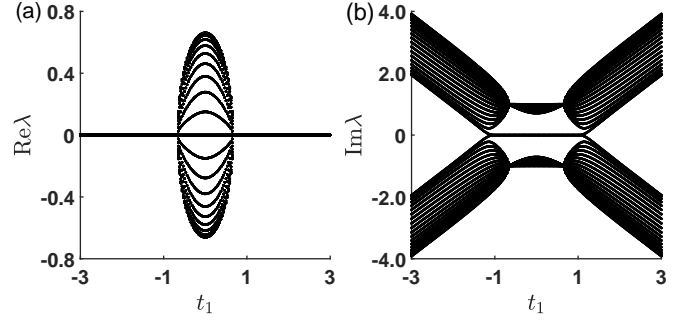


FIG. 9. (a-b) The real (a) and imaginary part (b) of numerical spectrum $\{\lambda\}$ of the shape matrix \mathbf{A}' with an open chain, here we choose $N = 20$, $t_2 = 1$, and $\gamma = 4/3$, t_1 varies from -3 to 3 .

seen that the edge states locate at $\text{Im}\lambda = 0$ (eightfold degenerate), ranging from $\left[-\sqrt{(\gamma/2)^2 + t_2^2}, \sqrt{(\gamma/2)^2 + t_2^2} \right]$, we also plot Fig. 4(c) as a comparison, while there show no edge states. From Fig. 4(e), there is one-to-one correspondence between the invariants and the boundary states, which indicates there exist a winding number with 0 or 4, and it matches the number of boundary states (0 or 8), because boundary states locate at each end of the system. For \mathbf{A} , by using Eq. (50), the total zak phase of the system $\sum_{\mu} \nu_{\mu}$ is 0 or 8π , thus the same conclusion holds. In summary, the bulk-edge correspondence preserves, which proves the validity and feasibility of our scheme.

VI. CONCLUSION

In this work, we develop a new approach to study the topological properties by utilizing the third quantization technique, and study an SSH lattice with collective loss and gain as an example. When quantum jumping terms are absent, by analyzing the property of the shape matrix, we find our scheme is consistent with the conventional approach in many aspects. In addition, the topological properties in the presence of quantum jumping terms are also studied. In this circumstance, due to the involvement of quantum jumps, the topological transition points may shift. Our work reveals the unique role of quantum jump terms between NH systems and master equations, which can not be neglected and explained by the effective Hamiltonian theory.

ACKNOWLEDGMENTS

We thanks Professor X.X.Yi for his helpful discussions. This work was supported by the National Natural Science Foundation of China (NSFC) under Grants No. 12175033, No. 12147206 and National Key R&D Program of China (No. 2021YFE0193500).

Appendix A: THE AZ SYMMETRY CLASSIFICATION

Class	A	AIII	AI	BDI	D	DIII	AII	CII	C	CI
T	0	0	+	+	0	-	-	-	0	+
C	0	0	0	+	+	+	0	-	-	-
S	0	1	0	1	0	1	0	1	0	1

TABLE I. AZ Classification of symmetries, T,C,S represent the symmetry of time reversal, particle hole and chiral. The 0 or 1 means the absence or presence of the symmetry, while the signs \pm indicate the $U_{T,C}U_{T,C}^* = \pm I$.

Appendix B: THE CALCULATION OF GENERALIZED BRILLOUIN ZONE

The calculation of the generalized Brillouin zone in the main text is basically based on the scheme proposed in Ref. [2, 13], where the usually used BZ in Hermitian case can be considered as its special circumstance. Here we give out a brief procedure for the calculation of GBZ.

(i) Suppose a 1D tight-binding model with total dimension $2M$, the Hamiltonian is given by

$$H = \sum_{n,i,\mu,\nu} t_{i,\mu\nu} c_{n+i,\mu}^\dagger c_{n,\nu}, \quad (\text{B1})$$

where n represents the n th cell of the model, μ, ν is the index of the fermion in an individual cell, which contains multiple degrees like momentum, spin, etc. t is the hopping strength and different i indicates the long-range interactions of lattices in different cells.

(ii) The eigen-function of Hamiltonian satisfies $H|\Psi\rangle = E|\Psi\rangle$, the eigenvector $|\Psi\rangle$ in the real space can be written as a linear combination

$$|\Psi\rangle = (\dots, \psi_{n,1}, \psi_{n,2} \dots \psi_{n+1,1} \dots)^T, \quad (\text{B2})$$

$$\psi_{n,\mu} = \sum_j \phi_{n,\mu}^{(j)} \phi_{n,\mu}^{(j)} = (\beta_j)^n \phi_{m,u}^{(j)}, \quad (\text{B3})$$

where Eq. (B3) is because of spatial periodicity.

(iii) After simplification, the characteristic equation of the Bloch form Hamiltonian $\mathcal{H}(\beta)$ can be presented as

$$f(\beta, E) = \det(\mathcal{H}(\beta) - E) = \frac{P(\beta, E)}{\beta^p} = 0, \quad (\text{B4})$$

where $\mathcal{H}(k)$ is performed by a substitution $e^{ik} \rightarrow \beta$. The norm of β is usually not necessarily unity, which is the reason why the ordinary Brillouin zone breaks down in NH cases. The p denotes the order of the pole of $P(\beta, E)$, and $f(\beta, E)$ can be trivially factorized as

$$f(\beta, E) = \prod_{\mu}^n (E - E_{\mu}(\beta)) = 0, \quad (\text{B5})$$

for multi bands, here n is the dimension of Bloch Hamiltonian \mathcal{H} .

(iv) Numerically calculate the eigenvalues E_i ($i=1,2,\dots,2M$) of H , and the β can be solved by function

$$f(\beta, E_i) = 0, \quad (\text{B6})$$

apparently, there are $2M$ solutions of β . To pick out the values of β , an important feature is the bulk-band property. For the solution labeled as $|\beta_1| \leq |\beta_2| \leq \dots \leq |\beta_{2M}|$, the continuum bands require a pair of β that satisfy

$$|\beta_M| = |\beta_{M+1}|, \quad (\text{B7})$$

which determine the trajectory of GBZ. In other word, there must exist a pair of conjugate points $\beta_M = \beta_0, \beta_{M+1} = \beta_0 e^{i\theta}$, where β_0 is a complex number. When H is Hermitian, it can be easily proved that GBZ is always a unit circle (Brillouin zone) [13].

Appendix C: THE MULTI GBZ CASES

With the help of *resultant*, we obtain the aGBZ of the shape matrix A' in Sec. IV, the next urgent task is to verify the actual area of GBZ. In Appendix B, we have known that the OBC spectrum $\{E\}$ is required in order to obtain the information of GBZ. However, we eliminate the degree E in Eq. (31), the values that can be taken from the energy spectrum $\{E\}$ is bounded, it may induce the GBZ usually a subset of aGBZ. To overcome this property, Ref. [50] puts up with the concept of a new kind of singularity point, self-conjugate points, that only occur in non-Hermitian systems, and the contours of aGBZ that possess the self-conjugate point must form GBZ. Recall that the Van Hove singularity k_s in Hermitian system [62], which satisfies

$$\partial_k E_{\mu}(k_s) = 0. \quad (\text{C1})$$

Since the β is an extension of k , the generalized critical points β_0 in NH system satisfy

$$\partial_k E_{\mu}(\beta_0) = 0. \quad (\text{C2})$$

In order to search the singularity points in all bands, we can use

$$f(E_0, \beta_0) = 0, \quad (\text{C3})$$

where E_0 satisfies

$$\begin{cases} f(E_0, \beta) = 0, \\ \frac{\partial f(E_0, \beta)}{\partial \beta} = 0, \end{cases} \quad (\text{C4})$$

it is proved that such self-conjugate points not only have $|\beta_M| = |\beta_{M+1}|$, but also $\beta_M = \beta_{M+1}$ [50].

-
- [1] Carl M. Bender, “Making Sense of Non-Hermitian Hamiltonians,” *Reports on Progress in Physics* **70**, 947–1018 (2007).
 - [2] Shunyu Yao and Zhong Wang, “Edge States and Topological Invariants of Non-Hermitian Systems,” *Physical Review Letters* **121**, 086803 (2018).
 - [3] Wen-Tan Xue, Yu-Min Hu, Fei Song, and Zhong Wang, “Non-Hermitian Edge Burst,” *Physical Review Letters* **128**, 120401 (2022).
 - [4] Zhihao Xu and Shu Chen, “Topological Bose-Mott insulators in one-dimensional non-Hermitian superlattices,” *Physical Review B* **102**, 035153 (2020).
 - [5] Tsuneya Yoshida, Koji Kudo, and Yasuhiro Hatsugai, “Non-Hermitian fractional quantum Hall states,” *Scientific Reports* **9**, 16895 (2019).
 - [6] Tony E. Lee, “Anomalous edge state in a non-hermitian lattice,” *Phys. Rev. Lett.* **116**, 133903 (2016).
 - [7] Kai Li and Yong Xu, “Non-hermitian absorption spectroscopy,” *Phys. Rev. Lett.* **129**, 093001 (2022).
 - [8] Emil J. Bergholtz, Jan Carl Budich, and Flore K. Kunst, “Exceptional Topology of Non-Hermitian Systems,” *Reviews of Modern Physics* **93**, 015005 (2021).
 - [9] Xiao-Ran Wang, Cui-Xian Guo, and Su-Peng Kou, “Defective edge states and number-anomalous bulk-boundary correspondence in non-Hermitian topological systems,” *Physical Review B* **101**, 121116 (2020).
 - [10] Chuanhao Yin, Hui Jiang, Linhu Li, Rong Lü, and Shu Chen, “Geometrical meaning of winding number and its characterization of topological phases in one-dimensional chiral non-Hermitian systems,” *Physical Review A* **97**, 052115 (2018).
 - [11] Ye Xiong, “Why does bulk boundary correspondence fail in some non-hermitian topological models,” *Journal of Physics Communications* **2**, 035043 (2018).
 - [12] Yuto Ashida, Zongping Gong, and Masahito Ueda, “Non-Hermitian physics,” *Advances in Physics* **69**, 249–435.
 - [13] Kazuki Yokomizo and Shuichi Murakami, “Non-Bloch Band Theory of Non-Hermitian Systems,” *Physical Review Letters* **123**, 066404 (2019).
 - [14] Crispin Gardiner, Peter Zoller, and Peter Zoller, *Quantum noise: a handbook of Markovian and non-Markovian quantum stochastic methods with applications to quantum optics* (Springer Science & Business Media, 2004).
 - [15] Fabrizio Minganti, Adam Miranowicz, Ravindra W. Chhajlany, and Franco Nori, “Quantum exceptional points of non-Hermitian Hamiltonians and Liouvillians: The effects of quantum jumps,” *Physical Review A* **100**, 062131 (2019).
 - [16] Kazuki Yamamoto, Masaya Nakagawa, Kyosuke Adachi, Kazuaki Takasan, Masahito Ueda, and Norio Kawakami, “Theory of Non-Hermitian Fermionic Superfluidity with a Complex-Valued Interaction,” *Physical Review Letters* **123**, 123601 (2019).
 - [17] Xiangyu Niu, Jianning Li, S. L. Wu, and X. X. Yi, “Effect of quantum jumps on non-Hermitian system,” *arXiv:2202.12591* (2022).
 - [18] Klaus Mølmer, Yvan Castin, and Jean Dalibard, “Monte Carlo wave-function method in quantum optics,” *Journal of the Optical Society of America B* **10**, 524 (1993).
 - [19] Andrew J. Daley, “Quantum trajectories and open many-body quantum systems,” *Advances in Physics* **63**, 77–149 (2014).
 - [20] Juan Mauricio Torres, “Closed-form solution of Lindblad master equations without gain,” *Physical Review A* **89**, 052133 (2014).
 - [21] Fei Song, Shunyu Yao, and Zhong Wang, “Non-Hermitian skin effect and chiral damping in open quantum systems,” *Physical Review Letters* **123**, 170401 (2019).
 - [22] Stefano Longhi, “Unraveling the non-Hermitian skin effect in dissipative systems,” *Physical Review B* **102**, 201103 (2020).
 - [23] Tsuneya Yoshida, Koji Kudo, Hosho Katsura, and Yasuhiro Hatsugai, “Fate of fractional quantum Hall states in open quantum systems: Characterization of correlated topological states for the full Liouvillian,” *Physical Review Research* **2**, 033428 (2020).
 - [24] Wei Nie, Mauro Antezza, Yu-xi Liu, and Franco Nori, “Dissipative Topological Phase Transition with Strong System-Environment Coupling,” *Physical Review Letters* **127**, 250402 (2021).
 - [25] Clemens Gneiting, Akshay Koottandavida, A. V. Rozhkov, and Franco Nori, “Unraveling the topology of dissipative quantum systems,” *Physical Review Research* **4**, 023036 (2022).
 - [26] C-E Bardyn, M A Baranov, C V Kraus, E Rico, A İmamoğlu, P Zoller, and S Diehl, “Topology by dissipation,” *New Journal of Physics* **15**, 085001 (2013).
 - [27] Felix Dangel, Marcel Wagner, Holger Cartarius, Jörg Main, and Günter Wunner, “Topological invariants in dissipative extensions of the Su-Schrieffer-Heeger model,” *Physical Review A* **98**, 013628 (2018).
 - [28] Fabrizio Minganti, Adam Miranowicz, Ravindra W. Chhajlany, Ievgen I. Arkhipov, and Franco Nori, “Hybrid-Liouvillian formalism connecting exceptional points of non-Hermitian Hamiltonians and Liouvillians via postselection of quantum trajectories,” *Physical Review A* **101**, 062112.
 - [29] Stephan Dürr, Juan José García-Ripoll, Niels Syassen, Dominik M Bauer, Matthias Lettner, J Ignacio Cirac, and Gerhard Rempe, “Lieb-liniger model of a dissipation-induced tonkgirardeau gas,” *Physical Review A* **79**, 023614 (2009).
 - [30] Yuto Ashida, Shunsuke Furukawa, and Masahito Ueda, “Quantum critical behavior influenced by measurement backaction in ultracold gases,” *Physical Review A* **94**, 053615 (2016).
 - [31] Zongping Gong, Sho Higashikawa, and Masahito Ueda, “Zeno Hall Effect,” *Physical Review Letters* **118**, 200401.
 - [32] Zongping Gong, Yuto Ashida, Kohei Kawabata, Kazuaki Takasan, Sho Higashikawa, and Masahito Ueda, “Topological Phases of Non-Hermitian Systems,” *Physical Review X* **8**, 031079 (2018).
 - [33] A. McDonald, R. Hanai, and A. A. Clerk, “Nonequilibrium stationary states of quantum non-Hermitian lattice models,” *Physical Review B* **105**, 064302 (2022).
 - [34] Fan Yang, Qing-Dong Jiang, and Emil J Bergholtz, “Liouvillian skin effect in an exactly solvable model,” *Physical Review Research* **4**, 023160 (2022).
 - [35] Tomaž Prosen, “Third quantization: A general method to solve master equations for quadratic open Fermi systems,” *New Journal of Physics* **10**, 043026 (2008).
 - [36] Alan A. Dzhiboev and D. S. Kosov, “Nonequilibrium perturbation theory in Liouville-Fock space for inelastic electron transport,” *Journal of Physics: Condensed Matter* **24**, 225304 (2012).
 - [37] Manfred Schmutz, “Real-time green’s functions in many body problems,” *Zeitschrift für Physik B Condensed Matter* **30**, 97–106 (1978).
 - [38] Konstantin G. Zloshchastiev and Alessandro Sergi, “Comparison and unification of non-Hermitian and Lindblad approaches with applications to open quantum optical systems,” *Journal of*

- Modern Optics* **61**, 1298–1308 (2014).
- [39] Alexander Altland and Martin R. Zirnbauer, “Nonstandard symmetry classes in mesoscopic normal-superconducting hybrid structures,” *Physical Review B* **55**, 1142–1161 (1997).
 - [40] Alexei Kitaev, “Periodic table for topological insulators and superconductors,” in *AIP conference proceedings*, Vol. 1134 (American Institute of Physics, 2009) pp. 22–30.
 - [41] Shinsei Ryu, Andreas P. Schnyder, Akira Furusaki, and Andreas W. W. Ludwig, “Topological insulators and superconductors: Tenfold way and dimensional hierarchy,” *New Journal of Physics* **12**, 065010 (2010).
 - [42] Simon Lieu, Max McGinley, and Nigel R. Cooper, “Tenfold Way for Quadratic Lindbladians,” *Physical Review Letters* **124**, 040401 (2020).
 - [43] Yan He and Chih-Chun Chien, “Topological classifications of quadratic bosonic excitations in closed and open systems with examples,” *Journal of Physics: Condensed Matter* **34**, 175403 (2022).
 - [44] Shunyu Yao, Fei Song, and Zhong Wang, “Non-hermitian chern bands,” *Physical review letters* **121**, 136802 (2018).
 - [45] Flore K. Kunst, Elisabet Edvardsson, Jan Carl Budich, and Emil J. Bergholtz, “Biorthogonal Bulk-Boundary Correspondence in Non-Hermitian Systems,” *Physical Review Letters* **121**, 026808 (2018).
 - [46] Kohei Kawabata, Nobuyuki Okuma, and Masatoshi Sato, “Non-Bloch band theory of non-Hermitian Hamiltonians in the symplectic class,” *Physical Review B* **101**, 195147 (2020).
 - [47] Deguang Wu, Jiao Xie, Yao Zhou, and Jin An, “Connections between the open-boundary spectrum and the generalized Brillouin zone in non-Hermitian systems,” *Physical Review B* **105**, 045422 (2022).
 - [48] Kai Zhang, Zhesen Yang, and Chen Fang, “Correspondence between winding numbers and skin modes in non-hermitian systems,” *Physical Review Letters* **125**, 126402 (2020).
 - [49] Gang-Feng Guo, Xi-Xi Bao, and Lei Tan, “Non-Hermitian bulk-boundary correspondence and singular behaviors of generalized Brillouin zone,” *New Journal of Physics* **23**, 123007 (2021).
 - [50] Zhesen Yang, Kai Zhang, Chen Fang, and Jiangping Hu, “Non-Hermitian Bulk-Boundary Correspondence and Auxiliary Generalized Brillouin Zone Theory,” *Physical Review Letters* **125**, 226402 (2020).
 - [51] Makio Kawasaki, Ken Mochizuki, and Hideaki Obuse, “Topological phases protected by shifted sublattice symmetry in dissipative quantum systems,” *Physical Review B* **106**, 035408 (2022).
 - [52] Ching-Kai Chiu, Jeffrey C. Y. Teo, Andreas P. Schnyder, and Shinsei Ryu, “Classification of topological quantum matter with symmetries,” *Reviews of Modern Physics* **88**, 035005 (2016).
 - [53] Ananya Ghatak and Tanmoy Das, “New topological invariants in non-Hermitian systems,” *Journal of Physics: Condensed Matter* **31**, 263001 (2019).
 - [54] Ruel Churchill and James Brown, *Ebook: Complex Variables and Applications* (McGraw Hill, 2014).
 - [55] J. Zak, “Berry’s phase for energy bands in solids,” *Physical Review Letters* **62**, 2747–2750 (1989).
 - [56] Yasuhiro Hatsugai, “Quantized Berry Phases as a Local Order Parameter of a Quantum Liquid,” *Journal of the Physical Society of Japan* **75**, 123601 (2006).
 - [57] Dorje C. Brody, “Biorthogonal quantum mechanics,” *Journal of Physics A: Mathematical and Theoretical* **47**, 035305 (2014).
 - [58] Masatoshi Sato, Kazuki Hasebe, Kenta Esaki, and Mahito Kohmoto, “Time-Reversal Symmetry in Non-Hermitian Systems,” *Progress of Theoretical Physics* **127**, 937–974 (2012), arXiv:1106.1806 [cond-mat, physics:math-ph, physics:quant-ph].
 - [59] J.C. Garrison and E.M. Wright, “Complex geometrical phases for dissipative systems,” *Physics Letters A* **128**, 177–181 (1988).
 - [60] G. Nenciu and G. Rasche, “On the adiabatic theorem for nonself-adjoint Hamiltonians,” *Journal of Physics A: Mathematical and General* **25**, 5741–5751 (1992).
 - [61] J. M. Zhang and R. X. Dong, “Exact diagonalization: The Bose–Hubbard model as an example,” *European Journal of Physics* **31**, 591–602 (2010).
 - [62] Léon Van Hove, “The occurrence of singularities in the elastic frequency distribution of a crystal,” *Phys. Rev.* **89**, 1189–1193 (1953).